Article

Cell Reports

Manipulation of Mitochondria Dynamics Reveals Separate Roles for Form and Function in Mitochondria Distribution

Graphical Abstract

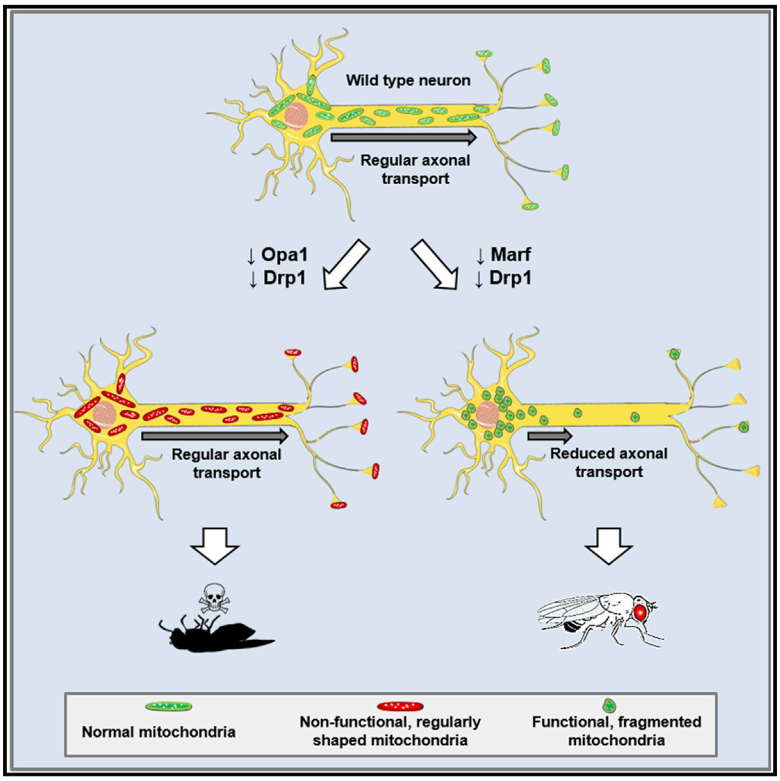

Authors

Tatiana Trevisan, Diana Pendin, Aldo Montagna, Sergio Bova, Anna Maria Ghelli, Andrea Daga

Correspondence

andrea.daga@gmail.com

In Brief

Trevisan et al. separate the independent contribution of form and function in determining the distribution of mitochondria in axons. They show that morphology is crucial for proper axonal mitochondria distribution, independent of their bioenergetic efficiency. However, the health of neurons depends on mitochondria function, but does not depend on shape or distribution.

Highlights

- Fragmention impairs mitochondria function and axonal distribution, leading to lethality
- Rescue of fragmentation restores mitochondria axonal distribution, but not viability
- Rescue of mitochondria function improves viability, independent of distribution

Trevisan et al., 2018, Cell Reports *23*, 1742–1753
May 8, 2018
https://doi.org/10.1016/j.celrep.2018.04.017

CellPress

OPEN ACCESS
CellPress

Cell Reports
Article

Manipulation of Mitochondria Dynamics Reveals Separate Roles for Form and Function in Mitochondria Distribution

Tatiana Trevisan,[1,4] Diana Pendin,[1,4,5] Aldo Montagna,[1] Sergio Bova,[2] Anna Maria Ghelli,[3] and Andrea Daga[1,6,*]
[1]Laboratory of Molecular Biology, Scientific Institute IRCCS E. Medea, Bosisio Parini, Lecco, Italy
[2]Department of Pharmaceutical and Pharmacological Sciences, University of Padova, Padova, Italy
[3]Department of Pharmacy and Biotechnology, University of Bologna, 40127 Bologna, Italy
[4]These authors contributed equally
[5]Present address: Department of Biomedical Sciences, University of Padova, 35131 Padova, Italy
[6]Lead Contact
*Correspondence: andrea.daga@gmail.com
https://doi.org/10.1016/j.celrep.2018.04.017

SUMMARY

Mitochondria shape is controlled by membrane fusion and fission mediated by mitofusins, Opa1, and Drp1, whereas mitochondrial motility relies on microtubule motors. These processes govern mitochondria subcellular distribution, whose defects are emphasized in neurons because of their polarized structure. We have studied how perturbation of the fusion/fission balance affects mitochondria distribution in *Drosophila* axons. Knockdown of Marf or Opa1 resulted in progressive loss of distal mitochondria and in a distinct oxidative phosphorylation and membrane potential deficit. Downregulation of Drp1 rescued the lethality and bioenergetic defect caused by neuronal Marf RNAi, but induced only a modest restoration of axonal mitochondria distribution. Surprisingly, Drp1 knockdown rescued fragmentation and fully restored aberrant distribution of axonal mitochondria produced by Opa1 RNAi; however, Drp1 knockdown did not improve viability or mitochondria function. Our data show that proper morphology is critical for proper axonal mitochondria distribution independent of bioenergetic efficiency. The health of neurons largely depends on mitochondria function, but does not depend on shape or distribution.

INTRODUCTION

Mitochondria are organelles present in all eukaryotic cells and preside over a wide variety of crucial functions, including respiration and energy production. Mitochondria are organized in a fluidly interconnected, dynamic network, and their structure and position are not fixed but vary by cell type, developmental stage, and physiological context. The dynamic behavior of the network is important for mitochondria distribution and inheritance; is important for remodeling during development and coordination of cell death programs; and allows cells to respond to shifting needs at different intracellular locations (Westermann, 2012).

Mitochondrial fusion and fission control the shape of mitochondria. The molecular machines that mediate mitochondrial division and fusion are dynamin-related proteins. Drp1 drives the scission of mitochondrial membranes and Mfn1/2 and Opa1 mediate fusion of the outer and inner mitochondrial membranes, respectively (Westermann, 2008). The motility of mitochondria within the cell depends on the action of microtubule-based motors (Lin and Sheng, 2015; Sheng, 2014). An ensemble of fission, fusion, and motility governs the distribution of mitochondria within the cell. This is especially evident in neurons whose polarized structure, which is characterized by the presence of axons and dendrites, emphasizes defects in the distribution of mitochondria. A growing body of evidence suggests that fusion and fission affect spatial distribution of mitochondria in neurons. Loss of Drp1, Marf/MFN, or Opa1 in *Drosophila* depletes mitochondria from neuromuscular junction synapses and motor axons (Sandoval et al., 2014; Verstreken et al., 2005; Yu et al., 2016). Mutations of the mitochondrial outer membrane fusion protein Mfn2 (Misko et al., 2012) or the inner membrane fusion protein Opa1 (Spinazzi et al., 2008) change the distribution of axonal mitochondria, and knockdown of Opa1 causes redistribution of dendritic mitochondria (Bertholet et al., 2013). It also has been proposed that a direct interaction exists between Mfn2 and the molecular machinery of mitochondrial transport (Baloh et al., 2007; Misko et al., 2010).

In addition to shape and distribution, the impact of alterations in the activity of mitochondrial dynamics proteins also resonates in mitochondrial function. Substantial evidence has been obtained in mammalian cells, indicating that loss of Mfn2 and Mfn1 function causes alterations in mitochondrial metabolism with loss of mitochondrial membrane potential and reduced endogenous respiration (Chen et al., 2005). Furthermore, Opa1 knockdown causes a widespread loss of mitochondrial membrane potential and a reduction in basal respiration (Chen et al., 2005; Olichon et al., 2003). The general tenet is that interconnected mitochondrial networks are found in respiratory active cells, whereas small and fragmented mitochondria are more prevalent in respiratory inactive cells (Westermann, 2012).

A number of biologically relevant questions thus arise. How are morphology and function linked to the subcellular distribution of mitochondria? Since it is thought that metabolically dysfunctional mitochondria are transported to the neuron body for clearance, is decreased respiration and the consequent retrograde transport of mitochondria triggered by fusion/fission defects responsible for aberrant distribution of axonal mitochondria? Is abnormal mitochondria morphology resulting from fusion/fission defects the reason for this aberrant distribution? Are morphology and function always linked? Do they together contribute to abnormal mitochondria transport? These questions carry also key medical relevance as mutations in Mfn2, Opa1, and Drp1 cause hereditary neuropathies (Burté et al., 2015; Pareyson et al., 2015) whose pathophysiologic mechanism has been proposed to be abnormal transport and distribution of mitochondria, leading to distal axonal degeneration (Misko et al., 2012).

We have examined *in vivo* how tweaking mitochondria fusion/fission balance perturbs mitochondria morphology and function and how these perturbations affect the distribution of mitochondria within *Drosophila* segmental nerves. We found that downregulation of Marf or Opa1 results in depletion of mitochondria at the neuromuscular junction synapse and in progressive distal loss of mitochondria along the extended axons in segmental nerves, but not in shorter photoreceptor axons. This effect was accompanied by a marked oxidative phosphorylation deficit. Simultaneous downregulation of Drp1 rescues the lethality and bioenergetic defect caused by neuronal Marf RNAi alone but ameliorates very marginally the distribution of axonal mitochondria. However, downregulation of Drp1 rescues fragmentation and aberrant distribution of axonal mitochondria induced by Opa1 RNAi without restoring viability or oxidative phosphorylation. Thus, our data show that shape is crucial for proper axonal mitochondria distribution, which in turn is largely independent of bioenergetic efficiency. However, the health of neurons depends on mitochondria function even in spite of irregular morphology and distribution. This has additional implications for mitochondria dynamics-dependent pathologies because it indicates that deficiencies observed in the absence of fusion/fission components may primarily arise from impaired mitochondrial function rather than disturbed mitochondrial transport and distribution.

RESULTS

We took advantage of the known impact of altered fusion/fission dynamics to address how morphology and function affect the axonal distribution of mitochondria. To this end, we used two available transgenic fly lines for *in vivo* RNAi-mediated knockdown of Opa1 or Marf, the fly orthologs of Opa1 and mitofusin 1/2, respectively. We validated and quantitated the efficiency of knockdown by real-time PCR on total RNA extracted from tubulin-Gal4/UAS-Marf-RNAi or UAS-Opa1-RNAi/+; tubulin-Gal4/+ second-instar larvae that express RNAi ubiquitously. This analysis shows that the expression levels of Marf and Opa1 were reduced by 84.5% ± 5.5% and 66.5% ± 9.7%, respectively (Figure S1). Morphology of mitoGFP-labeled neuronal mitochondria was evaluated within the cell bodies of ventral nerve cord neurons and segmental nerves of *Drosophila* third-instar larvae after expressing UAS-Marf-RNAi or UAS-Opa1-RNAi specifically in the nervous system using the elav-Gal4 driver. As expected (Debattisti et al., 2014; Sandoval et al., 2014; Yarosh et al., 2008; Yu et al., 2016), downregulation of either Marf or Opa1 causes distinct mitochondrial fragmentation. Fragmented mitochondria aggregate in the neuronal cell bodies of the ventral nerve cord (Figure 1A) and appear fragmented along segmental nerves (Figure 1B). Efficiency of knockdown was also confirmed by the observation that ubiquitous downregulation of Marf and Opa1 caused lethality at the second-instar and the immature third-instar larvae stages, respectively. In addition, neuron-specific downregulation of both genes resulted in late pupa lethality with a small percentage of ailing escapers that died soon after eclosion.

A dominant-negative allele of Drp1 has been shown to restore tubular mitochondria morphology in mitofusin mutant cells (Chen et al., 2003). We therefore tested whether fragmentation induced by loss of membrane fusion mediators Marf or Opa1 could be recuperated by concurrently inhibiting mitochondria fission. We selected an RNAi line that abates Drp1 levels sufficiently to induce an elongation phenotype (Figures S1 and S2) without however triggering the lethality associated with severe loss of Drp1 function (Verstreken et al., 2005) and expressed it under the control of the neuronal driver elav-Gal4 in combination with Opa1 RNAi or Marf RNAi. Downregulation of Drp1 in Marf RNAi flies did not restore mitochondrial shape (Figures 1A and 1B) but unexpectedly led to a significant rescue of the lethality elicited by Marf downregulation in the nervous system (Figure 2A). Eclosed elav-Gal4/UAS-Marf-RNAi,UAS-Drp1-RNAi individuals were in good conditions, had normal locomotor abilities, were fertile, and lived for weeks. Furthermore, unlike tubulin-Gal4/UAS-Marf-RNAi that barely reached the second-instar larva stage, tubulin-Gal4/UAS-Marf-RNAi,UAS-Drp1-RNAi larvae extended their development through to late third-instar stages. In contrast, neuronal downregulation of Drp1 in Opa1 RNAi flies resulted in an essentially wild-type mitochondrial morphology; neuronal cell bodies and segmental nerves displayed normally shaped mitochondria (Figures 1A and 1B). However, the lethality caused by neuronal or ubiquitous Opa1 knockdown was not rescued by co-expression of Drp1 RNAi (Figure 2A).

Because perturbation of the activity of mitochondrial dynamics proteins is known to affect also mitochondria function (Burté et al., 2015; Westermann, 2012; Yu et al., 2015), a possible explanation for our observations is that, despite the absence of morphological rescue, Drp1 downregulation restores proper mitochondrial function in Marf RNAi individuals leading to their survival. To verify this hypothesis, we evaluated mitochondrial function upon knockdown of Opa1 or Marf alone and in combination with knockdown of Drp1. Total oxygen consumption in larvae, the rate of ATP synthesis in isolated mitochondria and mitochondrial membrane potential in larval muscles were chosen as the readout for overall mitochondria function (Brand and Nicholls, 2011). Analysis of mitochondrial respiratory capacity shows that in tubulin-Gal4/UAS-Marf-RNAi or UAS-Opa1-RNAi/+;tubulin-Gal4/+ individuals oxygen consumption was reduced compared to controls by approximately 40% and 50%, respectively (Figure 2C). Likewise, the rate of ATP synthesis was reduced approximately by 80% in

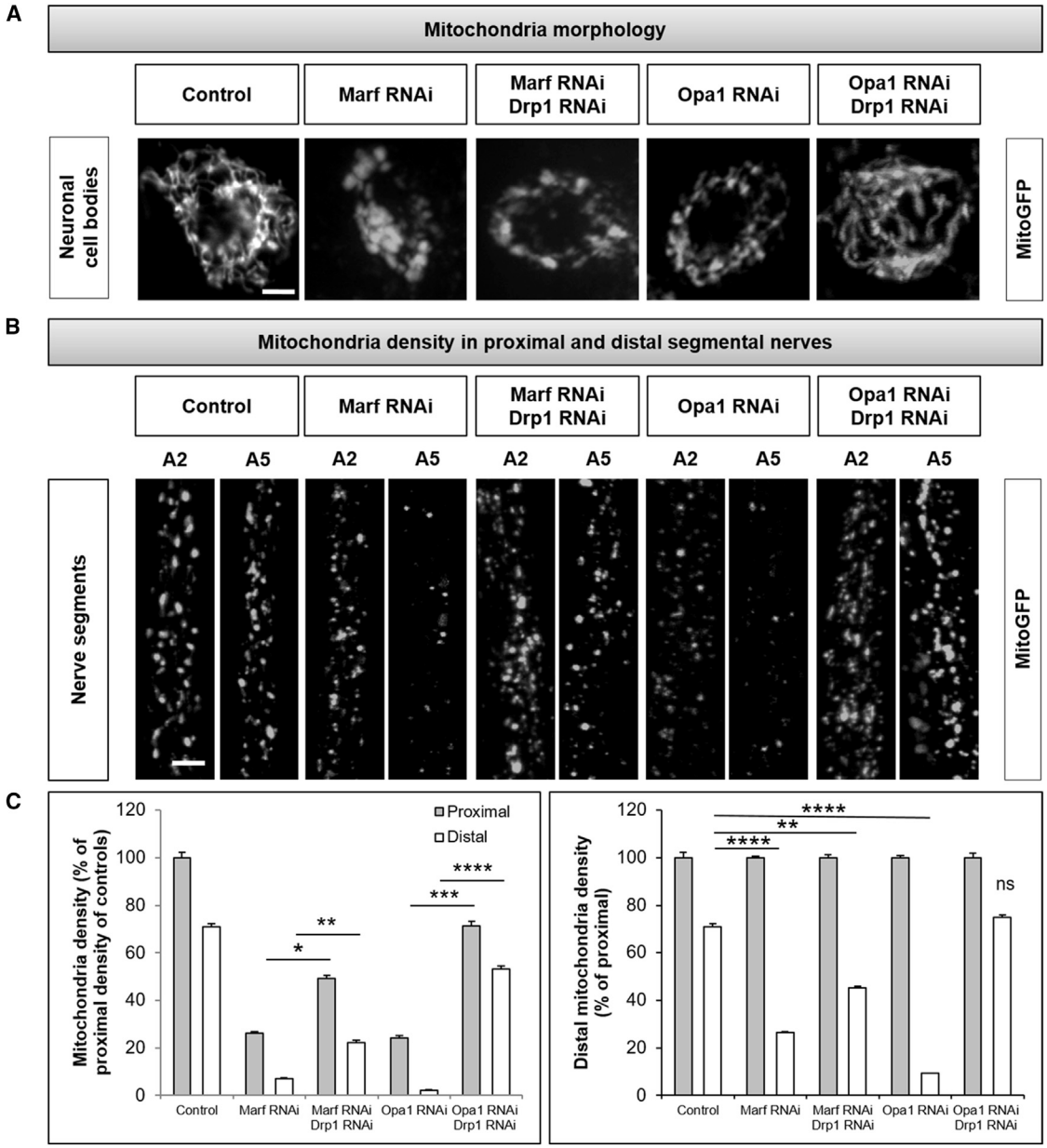

Figure 1. Mitochondria Morphology and Distribution in Axons

(A–C) Control and RNAi lines were crossed to the pan-neuronal driver elav-GAL4 and UAS-mitoGFP to label neuronal mitochondria. (A) Confocal images of third-instar larval neuronal cell bodies. Scale bar, 5 μm. (B) Confocal images of third-instar larva segmental nerves. For each genotype, a proximal (A2) and a distal (A5) section of the same nerve is shown. Scale bar, 5 μm. (C) The left bar graph shows for each experimental genotype the proximal and distal mitochondria densities normalized to the proximal density of controls; the right bar graph shows mitochondria density in the distal region of each genotype normalized to its corresponding proximal region.

Data are represented as mean ± SEM. n = 15, n (larvae) > 3.

tubulin-Gal4/UAS-Marf-RNAi and 60% in UAS-Opa1-RNAi/+; tubulin-Gal4/+ isolated mitochondria (Figure 2D). In further agreement, mitochondrial membrane potential measured with Rhodamine 123 (Scaduto and Grotyohann, 1999) was significantly reduced in both Mef-Gal4/UAS-Marf-RNAi and UAS-Opa1-RNAi/+;Mef-Gal4/+ larval muscle (Figure 3). These results confirm previous data indicating that disruption of outer or inner membrane fusion results in mitochondria dysfunction (Chen et al., 2005; Olichon et al., 2003). Importantly, the basal respiration deficit and loss of mitochondrial membrane potential associated with Marf knockdown were fully recovered upon simultaneous downregulation of Drp1 and the rate of ATP synthesis increased back to 56% ± 8% in double knockdowns compared to 23% ± 2% in single Marf knockdowns (Figures 2C and 2D).

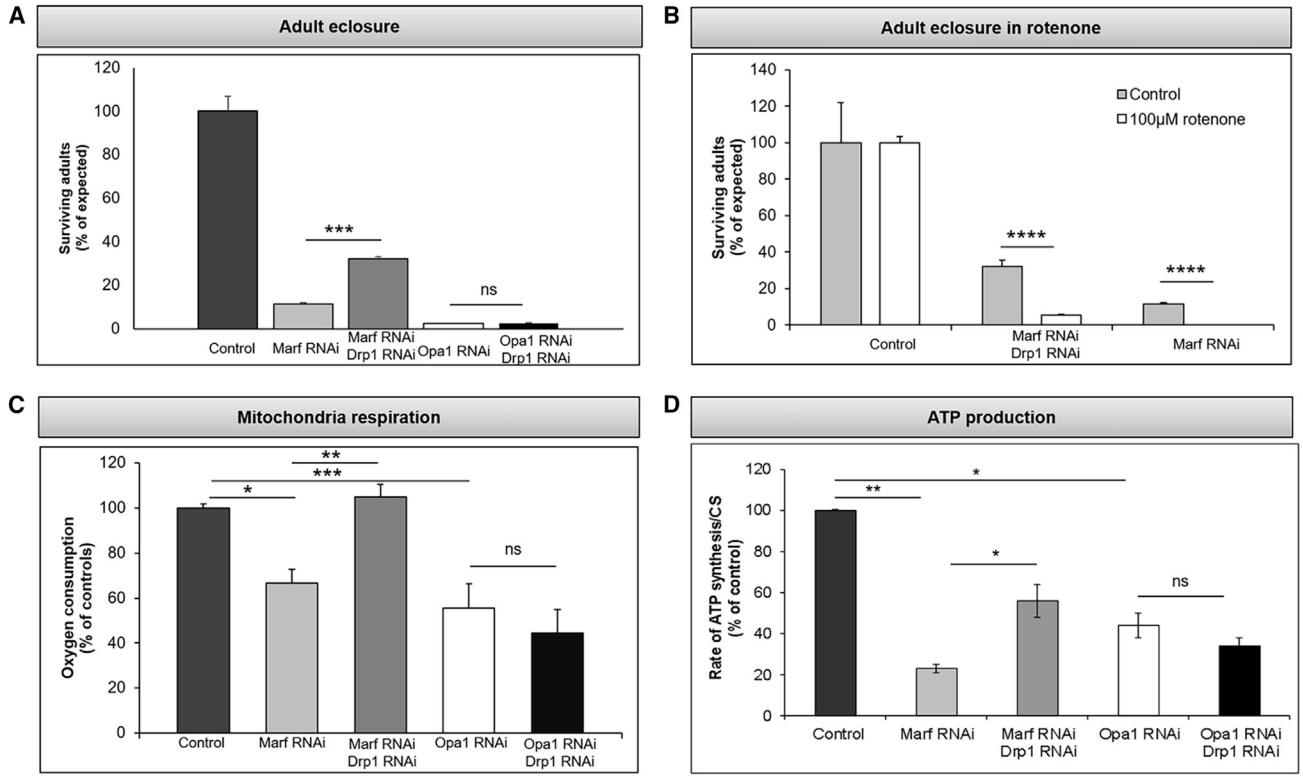

Figure 2. Viability and Mitochondria Function

(A) Quantification of eclosed adult flies of the indicated genotypic class expressed as the percentage of the expected. Controls and RNAi lines were crossed to the pan-neuronal driver elav-Gal4, and the number of adults for the expected genotypic classes was counted. Experiments were performed at 25°C.

(B) Quantification of adult eclosure for the indicated genotypes in the presence of rotenone.

(C) Mitochondria respiration assay. Control and RNAi lines were crossed to the ubiquitous driver tubulin-Gal4. Basal oxygen consumption was normalized to tissue weight. Data represent the mean of three independent experiments, and error bars indicate SEM.

(D) Control and RNAi lines were crossed to the ubiquitous driver tubulin-Gal4 and mitochondria were isolated. Rate of ATP synthesis driven by malate and pyruvate was normalized to protein content and CS activity. Histograms show the percentage of residual ATP synthesis respect to control.

Data represent the mean of three independent experiments ± SEM.

In contrast, in UAS-Opa1-RNAi/+;UAS-Drp1-RNAi/tubulin-Gal4 flies' oxygen consumption, rate of ATP synthesis, and membrane potential were reduced similar to Opa1 downregulation alone (Figures 2C and 2D), regardless of mitochondrial morphology. These data suggest a direct correlation, independent of mitochondria morphology, between rescue of viability and restoration of mitochondrial energetic efficiency. To assess whether viability correlates with oxphos functionality, we reasoned that inhibition of oxphos machinery should suppress the rescue of viability observed in elav-Gal4/UAS-Marf-RNAi,UAS-Drp1-RNAi flies. To inhibit oxphos, we grew elav-Gal4/UAS-Marf-RNAi,UAS-Drp1-RNAi and control flies on food containing 100 μM rotenone, the maximal concentration that allowed 100% survival of controls. We found that rotenone suppressed the rescue of viability of elav-Gal4/UAS-Marf-RNAi,UAS-Drp1-RNAi individuals (Figure 2B), demonstrating that the bioenergetic function of mitochondria mediates the rescue of viability.

Existing evidence intimates that manipulation of the levels of fission/fusion dynamics proteins alters mitochondria axonal distribution (Baloh et al., 2007; Misko et al., 2012; Sandoval et al., 2014; Verstreken et al., 2005; Yu et al., 2016). We have shown that downregulation of Opa1 or Marf *in vivo* in flies result in both morphological and functional mitochondria defects and established an experimental approach to uncouple mitochondria morphology and function. We thus went on to investigate the separate contribution of morphology and function on the distribution of mitochondria in neurons. We evaluated several parameters to identify axonal mitochondria distribution defects under Marf or Opa1 RNAi conditions. We first assessed mitochondria content at the neuromuscular junction (NMJ) on muscle 6/7 of segment A2 of UAS-Opa1-RNAi/+;elav-Gal4/+ and elav-Gal4/UAS-Marf-RNAi third-instar larvae by calculating the ratio between the volume of mitochondria at the synaptic terminal and the volume of the NMJ. Mitochondria were identified by mitoGFP fluorescence and axonal membranes were labeled using the neuronal marker horseradish peroxidase (HRP). Mitochondrial volume was chosen instead of number since loss of Marf or Opa1 reduces the average size of individual mitochondria possibly raising their overall number. A drastic reduction in mitochondria content was observed in NMJs lacking Marf (89% ± 0.25%) or Opa1 (95% ± 0.08%) (Figures 4A and 4B). Mitochondria distribution along the axon was then evaluated by measuring

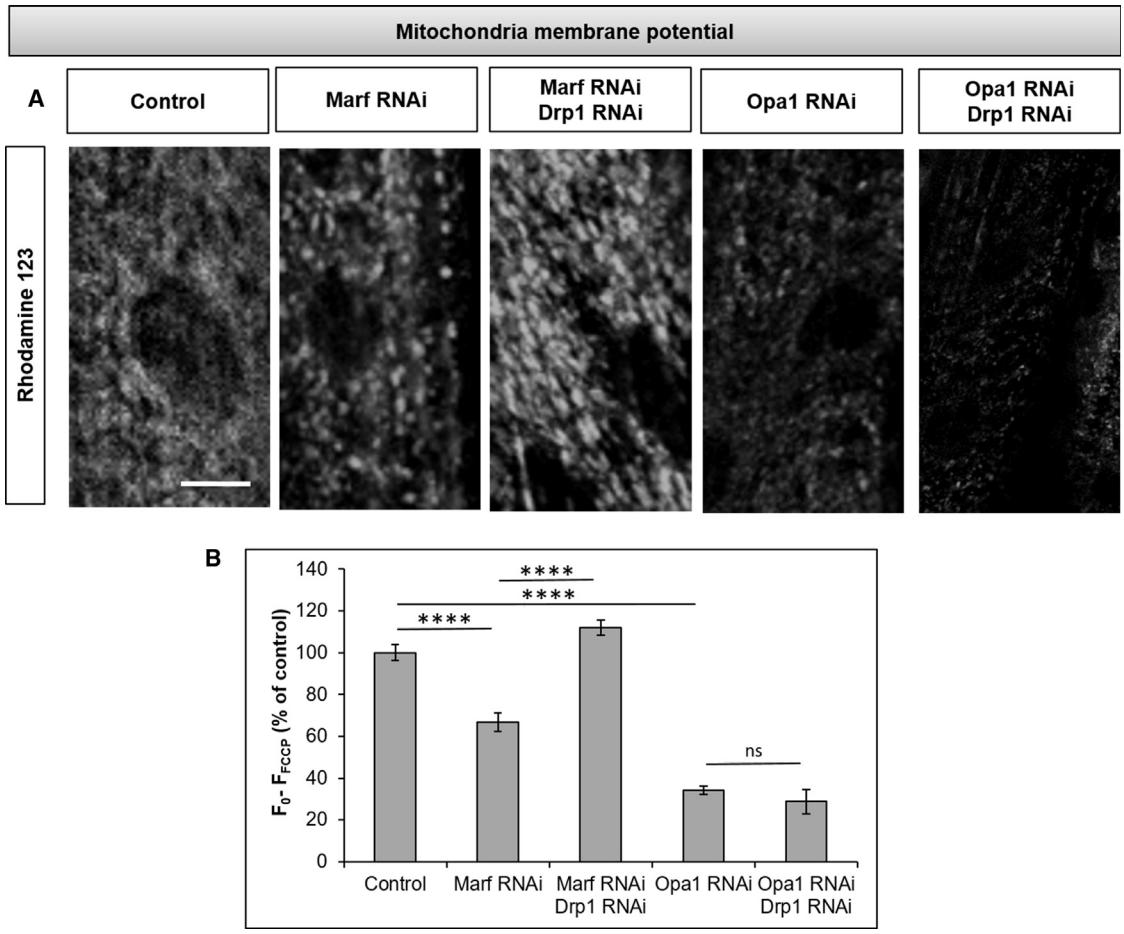

Figure 3. Mitochondria Membrane Potential Analysis

(A) Fluorescence images of third-instar larvae muscles expressing the indicated transgenes with Mef-GAL4 stained with Rhodamine 123. Scale bar, 10 μm.

(B) Fluorescence values for each genotype were calculated by subtracting fluorescence recorded 5 min after carbonyl cyanide 4-(trifluoromethoxy)phenylhydrazone (FCCP, 50 μm) addition (F_{FCCP}) from the initially measured fluorescence (F_0).

Data are represented as mean ± SEM n > 10, n (larvae) > 3.

mitochondrial density in the proximal (250 μm away from the cell bodies) and distal (1,500 μm away from the cell bodies) regions of segmental nerves of UAS-Opa1-RNAi/+;elav-Gal4/+ and elav-Gal4/UAS-Marf-RNAi third-instar larvae (Figures 1B and 1C). In these experimental genotypes we noticed a general reduction of mitochondria both proximally and distally compared to controls. Mitochondrial density in the distal region of control nerves was reduced by 60% of the density in the proximal region indicating that a small progressive loss of density is normal in long axons. However, this physiological decrease in density was robustly enhanced upon downregulation of Marf or Opa1. In fact, distal mitochondria density was about 10-fold lower in UAS-Opa1-RNAi/+;elav-Gal4/+ and about 5-fold lower in elav-Gal4/UAS-Marf-RNAi compared to the corresponding proximal densities (Figure 1C). Altogether, these data demonstrate that loss of inner or outer mitochondria membrane fusion causes impaired mitochondrial distribution along axons and suggest a length dependent impairment in mitochondrial positioning along the axon. To confirm this dependence, we analyzed mitochondria distribution in optic nerves, which are about 20-fold shorter than segmental nerves. We expressed Marf RNAi or Opa1 RNAi in the fly eye using the GMR-Gal4 driver and confirmed that downregulation of both proteins induces mitochondrial fragmentation (Figure S3). We then evaluated mitochondrial density in proximal (20 μm from the cell body) and distal (80 μm from cell body) regions of the optic nerve. No significant differences were observed between the mitochondrial densities in the proximal versus the distal regions of the axons (Figure S4), corroborating the notion that the defect in mitochondrial positioning observed in segmental nerve axons is length dependent and confirming that, also in flies, long axons are more prone to insult.

Recent studies have reported a physical interaction between MFN2 and the motor adaptor complex for mitochondria transport Miro, suggesting a direct involvement of mitofusin in mitochondria transport (Misko et al., 2010). We thus tested whether *Drosophila* Marf and Miro interact physically. Marf-myc and dMiro-EGFP were co-transfected in S2 cells and immunoprecipitated using anti-GFP (Figure S5). The absence of Marf-myc

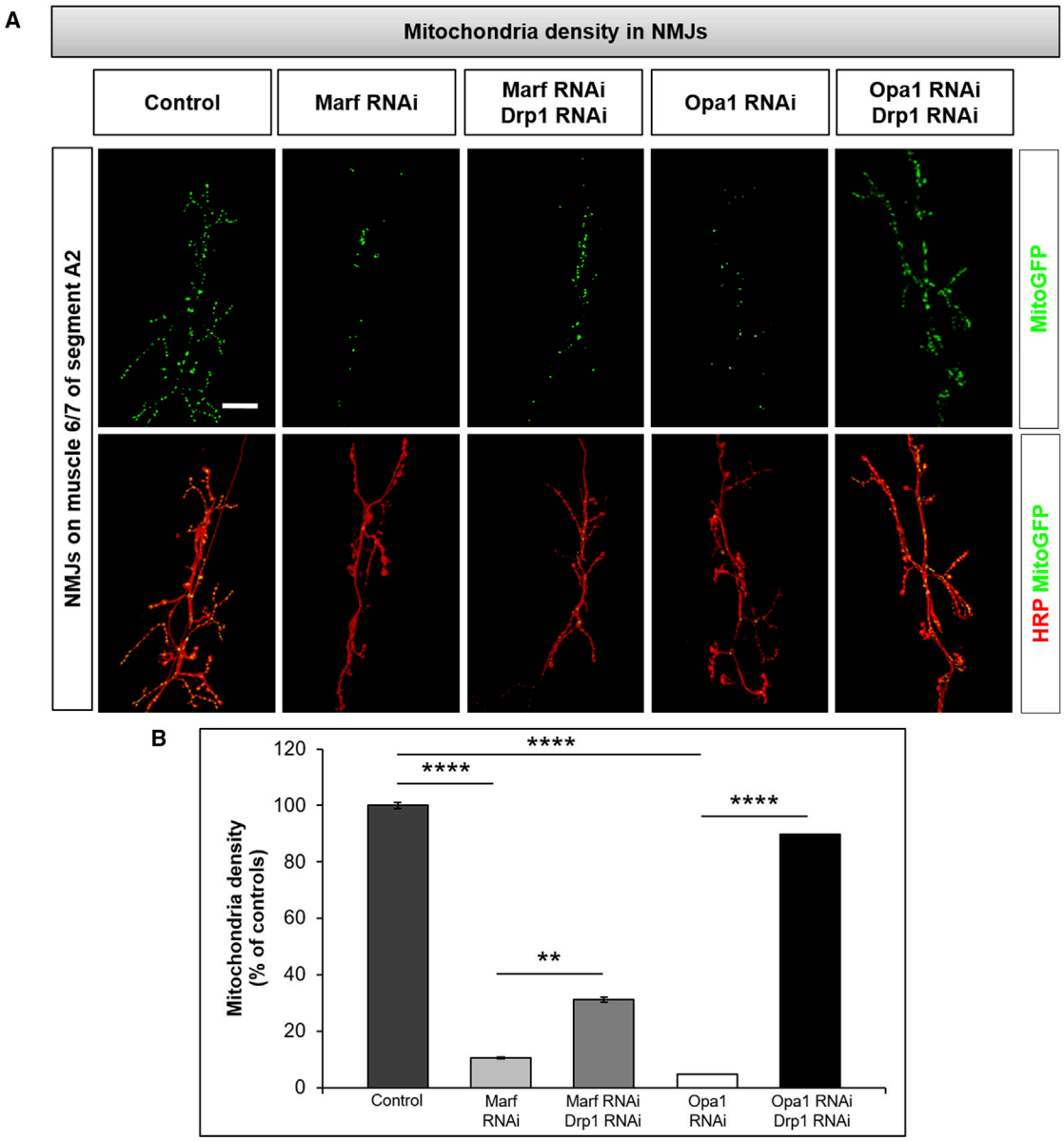

Figure 4. Mitochondria Distribution in NMJs

(A) Confocal images of third-instar larvae NMJs on muscles 6/7 of the A2 segment. Control and RNAi lines were crossed to the pan-neuronal driver elav-Gal4 and UAS-mitoGFP to label mitochondria. The upper panels show GFP labeling of mitochondria in NMJs of indicated genotypes. The lower panels show the same NMJs labeled with anti-HRP for identification. Scale bar, 20 μm.

(B) Quantification of mitochondria at NMJs. The volume of mitochondria in NMJs was normalized to the volume of HRP. n = 15, n (larvae) > 5. Data are represented as mean ± SEM.

signal in the pellet lane strongly suggest that these two proteins do not interact. Together with our *in vivo* data demonstrating that loss of axonal mitochondria is not a prerogative of Marf depletion as it occurs prominently also in the absence of Opa1, the co-immunoprecipitation (coIP) results indicate that, at least in *Drosophila*, mitofusin is not a component of the mitochondria transport machinery.

To explain axonal distribution impairment it has been proposed that disruption of mitochondria dynamics leads to the generation of dysfunctional mitochondria, which are retrogradely transported to the cell body to enter the autophagic pathway, leaving the cell periphery devoid of mitochondria (Cai et al., 2012; Miller and Sheetz, 2004). Other authors, however, did not find a correlation between mitochondrial membrane potential and the direction of motility (Verburg and Hollenbeck, 2008). Furthermore, the occurrence of local mitophagy in distal axons has also been reported (Ashrafi et al., 2014). We explored the possibility that an increase in

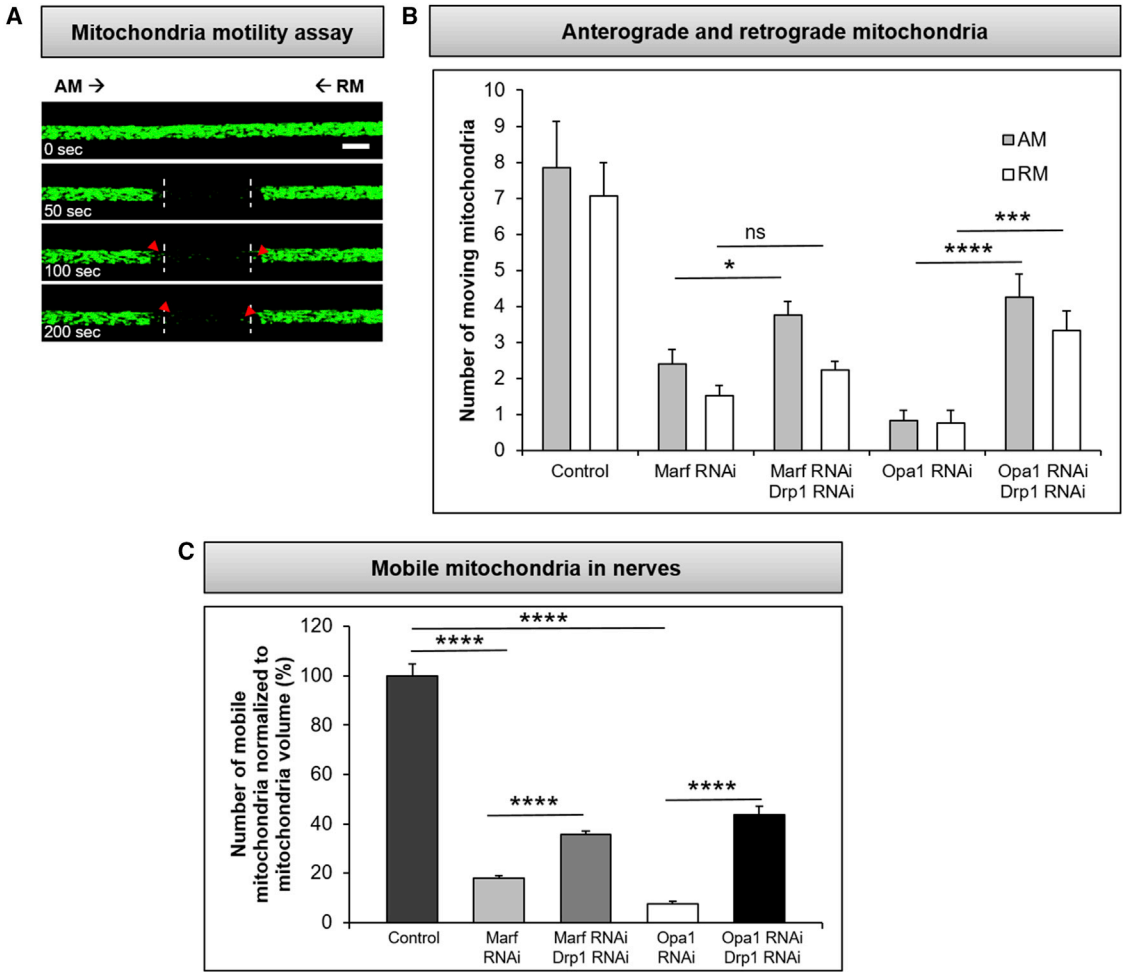

Figure 5. Mitochondria Motility in Axons

(A) Transport of mitochondria in wild-type segmental nerve axons. A series of confocal images from a time-lapse video of GFP-labeled mitochondria in the central region of a segmental nerve of third-instar larvae. A region of 40 μm was photobleached, and mitochondria entering the bleached region were counted. Anterograde and retrograde directions are indicated by arrows. Anterograde mitochondria (AM) enter the bleached area from the left boundary, and retrograde mitochondria (RM) enter from the right boundary. We considered only mitochondria that crossed the dotted line. Scale bar, 10 μm.

(B) Mean numbers of AM or RM entering the bleached region over 200 s. n = 18, n (larvae) > 6.

(C) Bar graph shows the percentage of moving mitochondria.

Data are represented as mean ± SEM.

retrograde trafficking under Marf and Opa1 RNAi conditions could explain the observed lack of distal mitochondria by analyzing mitochondria motility in UAS-Opa1-RNAi/+;elav-Gal4/+ and elav-Gal4/UAS-Marf-RNAi third-instar larvae. We determined the percentage and the absolute number of mobile mitochondria along a stretch of segmental nerve. Mobile mitochondria were tracked using mitoGFP and tallied after photobleaching a 40-μm segmental nerve section by counting the number of anterograde and retrograde mitochondria that entered the photobleached area over a 200 s period (Figure 5A). The percentage of mobile mitochondria was obtained by normalizing the number of mobile mitochondria to the volume of mitochondria present in the 40 μm nerve section before photobleaching. In UAS-Opa1-RNAi/+;elav-Gal4/+ and elav-Gal4/UAS-Marf-RNAi nerves we did not observe an increase in the number of retrograde mitochondria (Figure 5B). Nevertheless, we found that the percentage of mobile mitochondria (anterograde plus retrograde) was reduced in both Marf RNAi and more severely in Opa1 RNAi larvae (Figure 5C) indicating widespread impairment of mitochondria transport. These data suggest that distal loss of mitochondria is not due to increased retrograde transport of dysfunctional mitochondria to the cell body for clearance.

It is plausible that appropriate morphology is required for mitochondria to be correctly dispatched to neuronal processes and thus that shape may govern mitochondria mobility directly, independently of function. However, this direct link has remained elusive because usually changes in the bioenergetic state alter mitochondrial morphology and, conversely, disruption of mitochondrial morphology by genetic manipulation of fission and

fusion alters mitochondrial function (Yu et al., 2015). It has therefore been complex to separate experimentally the contribution of shape from that of function. Using our genetic paradigms, we asked whether the obvious trafficking defects seen in axonal mitochondria of Marf RNAi and Opa1 RNAi individuals could be recuperated by balancing loss of membrane fusion through the inhibition of fission. We analyzed the amount of mitochondria in the NMJs, as well as their proximal and distal densities along the nerves of UAS-Opa1-RNAi/+;UAS-Drp1-RNAi/elav-Gal4 and UAS-Marf-RNAi,UAS-Drp1-RNAi/elav-Gal4 individuals. A limited rescue of mitochondria density and distribution occurs in Marf-RNAi,Drp1-RNAi larvae (Figures 1B, 1C, 4A, and 4B) which display a substantial restoration of energetic efficiency (Figure 2) but still contain fragmented mitochondria. In contrast, mitochondrial density and distribution were broadly rescued in Opa1-RNAi;Drp1-RNAi larvae (Figures 1B, 1C, 4A, and 4B) where normally shaped mitochondria still display a severe energetic deficit (Figure 2). These results show that recovery of proper mitochondrial shape, but not restoration of oxidative phosphorylation, is sufficient to rescue mitochondria trafficking defects in axons. In other words, our data show that respiration-deficient mitochondria do not display positioning defects when they are properly shaped, thus suggesting that the energetic defect is likely not the cause of the distribution defect observed in Marf and Opa RNAi.

To gain further insights into the functional defects elicited by alterations of Marf, OPA1 and Drp1 we examined mitochondria in flight muscles of adult *Drosophila* expressing transgenic RNAi, individually or in combination, under the control of the muscle-specific driver Mef-Gal4. We chose this tissue because the size of mitochondria in muscles permits a meticulous analysis of their ultrastructure. We first verified whether expression of these transgenic RNAi in muscles, singly or in combination, paralleled the effects on viability produced by neuronal expression. These experiments showed that single muscle-specific expression of Marf or OPA1 RNAi resulted in lethality while Mef-Gal4/Drp1 RNAi individuals were viable. Co-expression of Drp1 and OPA1 RNAi in muscles remained lethal indicating that loss of Drp1 does not suppress the lethality caused by OPA1 RNAi. However, similar to neuronal expression, Drp1 RNAi was capable of rescuing substantially the lethality associated with muscle-specific Marf-RNAi. Because integrity of inner membrane organization is crucial for proper function, we examined the ultrastructure of mitochondria in the different genetic combinations by electron microscopy in muscles. Loss of Marf or OPA1 function leads to severe impairment of the internal ultrastructure of mitochondria that no longer display the typical organization in cristae of the inner membrane (Figure 6). Loss of Drp1 in the Opa1 RNAi background did not induce recovery of such internal organization and the interior space of mitochondria remained highly disordered. Interestingly, however, we found that when Drp1 was downregulated in the Marf RNAi background, 52% of mitochondria (n = 600) regained their normal ultrastructure, which is characterized by the presence of regular cristae arrays. This finding is consistent with our functional data showing a robust recovery of both respiratory activity and ATP production in UAS-Marf-RNAi,UAS-Drp1-RNAi/tubulin-Gal4 individuals.

DISCUSSION

The mitochondria fusion and fission machinery is essential for cells and genetic ablation of individual components in animal models results in death. The physiological relevance of fission/fusion processes also has become apparent from the study of patients harboring mutations in components of either fusion (Mfn2 and Opa1) or fission (Drp1) (Burté et al., 2015). The prime consequence of mutation or absence of fusion and fission proteins is a change in mitochondrial shape. Additionally, perturbation of mitochondrial transport and impairment of mitochondrial functions have frequently been reported (Wai and Langer, 2016; Westermann, 2012; Yu et al., 2015). Derangement of fusion/fission dynamics affects in particular neurons with the longest axons and high energetic requirements, such as peripheral sensory and motor neurons, because their considerable length demands proper mitochondria functioning and distribution along nerves. The pleiotropic array of mitochondrial dysfunctions that follows the loss of fusion/fission players challenges our ability to explain this observation. Are long axons more vulnerable because of disrupted mitochondrial trafficking, because mitochondrial function is impaired, or both?

In this work, we have investigated whether the spatial distribution of mitochondria along axons depends on form, function or both. We found that *in vivo* in *Drosophila* disruption of inner or outer membrane fusion caused by Opa1 and Marf knockdown, respectively, results in mitochondria fragmentation and in a severe oxidative phosphorylation deficit. We also observed a striking change in the spatial distribution pattern of axonal mitochondria in larval segmental nerves with a progressive loss of mitochondria along the axon in the distal direction. Distal loss was exacerbated in the NMJs that were essentially devoid of mitochondria. This defect was clearly length-dependent, as shorter photoreceptor axons did not display such phenotype, thus confirming that also in flies long axons are more prone to insult. Our data indicate that distal mitochondria loss is unlikely to occur because of increased transport back to the neuron body for the autophagic clearance of dysfunctional mitochondria since we found that downregulation of Opa1 or Marf heavily repressed trafficking in both the anterograde and retrograde directions. A specific role for Marf in linking mitochondria to the transport machinery through an interaction with Miro was also ruled out in flies, both because the two proteins did not coIP and because distal axonal loss is not specific for Marf but is observed after Opa1 knockdown and has been reported as a consequence of severe Drp1 mutation (Verstreken et al., 2005).

To directly address the importance of mitochondria morphology on axonal distribution we downregulated Drp1 in Marf or Opa1 depleted flies. We reasoned that achieving new fusion/fission equilibrium might rescue mitochondria shape and, consequently, the Marf RNAi and Opa1 RNAi phenotypes. Surprisingly, we found that rescue of Opa1 RNAi morphology defects by downregulation of Drp1 was associated with restoration of axonal mitochondria distribution. However, neither the bioenergetic capacity nor the lethality associated with Opa1 knockdown was rescued. In contrast, simultaneous downregulation of Marf and Drp1 led to a very robust rescue of lethality and strong restoration of oxidative phosphorylation. These double

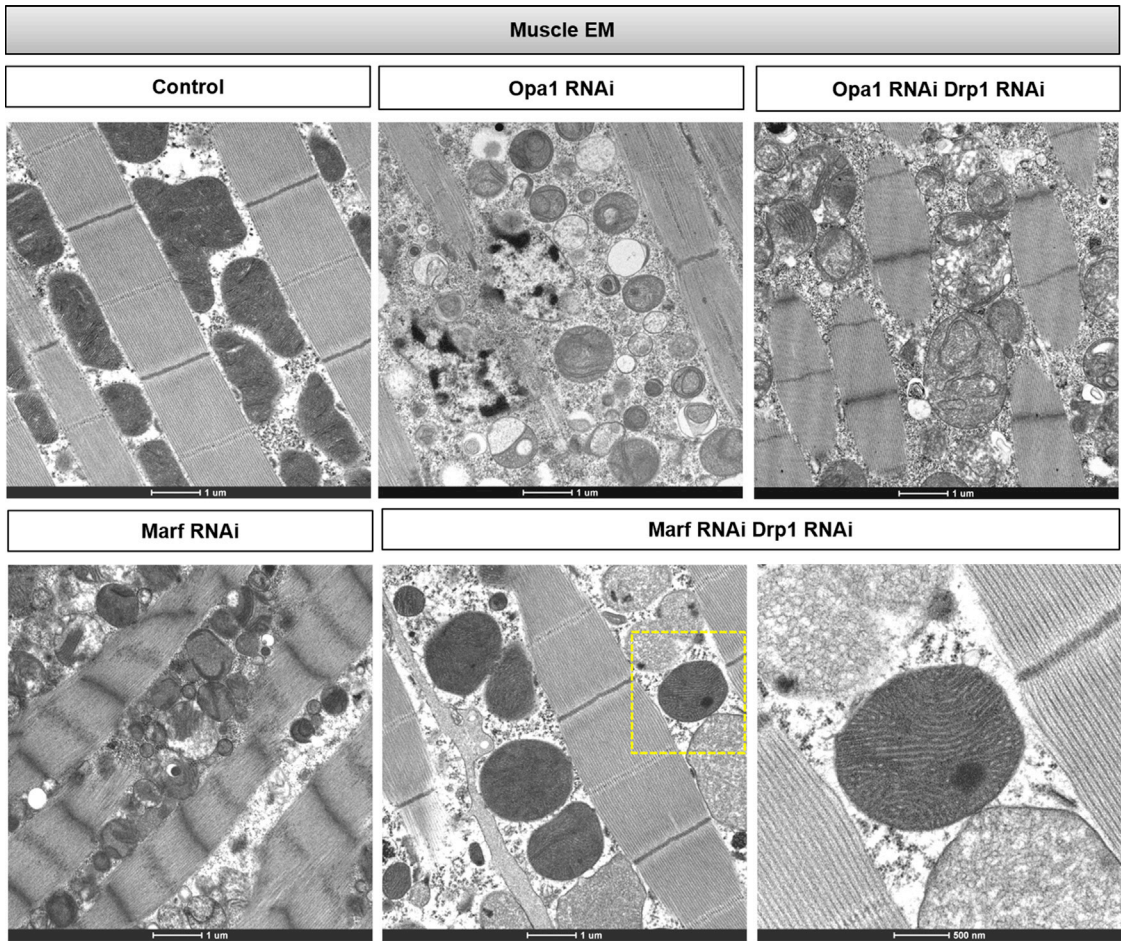

Figure 6. Mitochondria Ultrastructure in Adult Muscle

UAS-RNAi transgenes were expressed specifically in muscles using the Mef-Gal4 driver line. Representative EM images of indirect flight muscles are shown. The bottom right panel is an enlargement of the area boxed in yellow showing a mitochondrion with normal cristae organization.

RNAi individuals, however, had fragmented mitochondrial morphology and displayed very limited rescue of axonal mitochondria distribution, suggesting that shape is more critical than function for mitochondria transport. A plausible rationalization of these results could be that Opa1-RNAi;Drp1-RNAi mitochondria are more elongated because Marf continues to fuse the outer membrane while fission is inhibited, but remain dysfunctional because disruption of inner membrane cristae organization due to the absence of Opa1 (Meeusen et al., 2006) reduces their respiratory capacity (Chen et al., 2005; Olichon et al., 2003). Conversely, partial recovery of a balance between outer membrane fusion and fission in Marf-RNAi,Drp1-RNAi mitochondria only marginally restores morphology and distribution but is sufficient to support normal respiratory activity and considerably ameliorate oxidative phosphorylation. This interpretation is strongly supported by electron microscopy (EM) analysis, clearly demonstrating that Opa1-RNAi;Drp1-RNAi mitochondria display severely altered internal organization while over 50% of Marf-RNAi,Drp1-RNAi mitochondria display normal organization and ultrastructure fully resembling wild-type mitochondria.

Available data indicate that deficiency in protein components of the mitochondrial fusion machinery reduces mitochondrial membrane potential and respiration (Westermann, 2012; Zorzano et al., 2010), implying that altered mitochondrial morphology and perturbed function always go hand in hand. Here, we show that the consequences of mitochondria dysmorphology and dysfunction can be dissociated, suggesting that mitochondria shape and function do not necessarily have an obligatory relationship. In fact, fragmented mitochondria with essentially normal bioenergetics capability can be generated within the nervous system of a living *Drosophila*. These flies contain very few mitochondria in distal axons and NMJs, but they are viable because many of their mitochondria are functional. The fact that a small number of bioenergetically active mitochondria can support normal neuronal function should not come as a surprise. Indeed, recent studies have highlighted the importance of local glycolysis to meet energy demands at synapses (Jang et al., 2016; Rangaraju et al., 2014).

The genetic paradigms created have allowed us to separate the independent contribution of form and function in

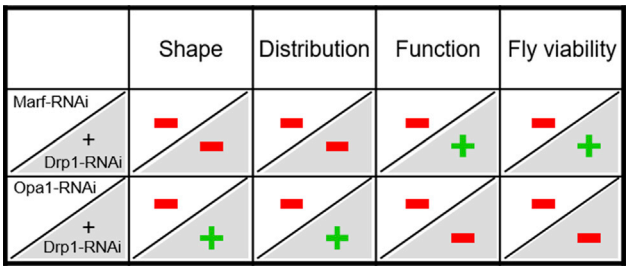

Figure 7. Schematic Representation of the Phenotypes Induced by Neuronal Expression of the Indicated RNAi Lines and Their Combinations

White areas display the effects of Marf or Opa1 downregulation alone; gray areas display the effects of Marf RNAi or Opa1 RNAi in combination with Drp1-RNAi. A red minus sign indicates impairment; a green plus sign indicates rescue of the impaired phenotype.

determining the subcellular distribution of mitochondria. Proper mitochondria distribution requires quasi-normal external mitochondria morphology; however, this is not sufficient to ensure proper neuronal function, which not unexpectedly, depends on normal mitochondrial metabolic activity (Figure 7). One possible explanation linking mitochondria shape to their distribution is that fragmented mitochondria may not provide proper anchoring for transport adaptor molecules that reside in the outer membrane, such as Miro/Milton. Perhaps a smaller size does not warrant attachment of a sufficient number of adaptors to the individual mitochondrion for its correct mobility. This would provide a reason restoration of shape rescues the distribution of metabolically inefficient axonal mitochondria.

We have generated an *in vivo* system in which mitochondria fragmentation is not accompanied by encumbering bioenergetic dysfunctions. Mitochondrial fragmentation is observed in a variety of pathological conditions (Burté et al., 2015; Pareyson et al., 2015; Schon and Przedborski, 2011), and our results indicate that in diseases characterized by altered mitochondrial morphology and altered axonal distribution, these defects may not be the primary cause of pathology since in our *Drosophila* model restoration of morphology and distribution without restoration of respiratory capacity does not permit survival.

EXPERIMENTAL PROCEDURES

Drosophila Genetics

Fly culture was performed using standard procedures. The *Drosophila* strains used were elav-Gal4; GMR-Gal4, tubulin-Gal4, and UAS-mito-GFP (Bloomington *Drosophila* stock center) and UAS-Drp1-RNAi (44155), UAS-Marf-RNAi (40478), and UAS-Opa1-RNAi (105706) (Vienna *Drosophila* RNAi Center). Control genotypes varied by individual experiments, but always included promoter-Gal4/+ individuals.

Rotenone Treatment

Serial dilutions of rotenone (Sigma, MO, USA) were made in dimethyl sulfoxide (DMSO, Sigma, MO, USA). Stocks or vehicle were added with vigorous mixing to molten cornmeal molasses agar media to a final concentration of 100 μM rotenone and 0.25% DMSO. Individuals of the desired genotypes were continuously exposed to the drug as parent flies laid fertilized eggs in rotenone-containing media.

RNA Isolation and Quantitative Real-Time PCR

The relative expression levels of Drp1, Marf, and Opa1 mRNAs were determined using quantitative real-time PCR. Total RNA was isolated from third-instar larvae with Direct-zol RNA MiniPrep (ZymoResearch) using standard protocols. The concentration and purity of RNA samples were determined using NanoDrop 2000c Spectrophotometer (ThermoScientific). Each RNA sample was amplified using One-Step SYBRR PrimeScript RT-PCR Kit II (Takara) in an Eco Real-Time PCR System (Illumina). The housekeeping RP49 gene was used as an internal control to normalize the data. Data represented are the result of three independent measurements run in triplicate. The gene specific primers are shown below:

RP49 For 5′-AGGCCCAAGATCGTGAAGAA-3′,
RP49 Rev 5′-TCGATACCCTTGGGCTTGC-3′,
Drp1 For 5′-TCCACAATCTTCTCGTGCAG-3′,
Drp1 Rev 5′-CATTCACGAGGAGATGCAGC-3′,
Marf For 5′-GTATGTCCATGAGACGACCA-3′,
Marf Rev 5′-CTTGTACACATAGCTTTCGA-3′,
Opa1 For 5′-GACTCTGACCGGGAATACGA-3′,
Opa1 Rev 5′-CTAGAACCATGCGTTGCAGA-3′.

Immunohistochemistry

Third-instar larvae raised at 28°C were harvested, dissected in PBS 1× (Lonza), fixed in 4% paraformaldehyde for 10 min, and washed in PBS containing 0.2% Triton X-100 (Sigma). Then larvae were incubated with a Cy3-conjugated anti-HRP antibody (1:500; Jackson ImmunoResearch Laboratories) overnight at 4°C. All confocal images were acquired using a confocal microscope (Nikon D-ECLIPSE C1) equipped with a Nikon 60× oil Plan Apochromat objective using the Nikon EZ-C1 acquisition software. Images were analyzed with Volocity (PerkinElmer Company, Santa Clara, CA, USA) or ImageJ.

Mitochondria Density Analysis

Larvae were dissected as previously described (Louie et al., 2008). To quantify mitochondria distribution, we compared mitochondrial density in 40-μm-long proximal and distal regions of the same segmental nerve. Mitochondria density was evaluated by collecting a series of confocal z stacks to determine the volume of mitochondria (volume of mito-GFP) and the volume of the nerve (volume enclosed by HRP fluorescence). The volume of mitochondria was normalized to the volume of the HRP-labeled nerve and the ratio between mitochondria density in distal region and mitochondria density in proximal region was calculated for each nerve. Mitochondria distribution in short axons was quantified in the same way, except that 5-μm-long proximal and distal regions of the optic nerve were considered.

Mitochondrial Membrane Potential Analysis

Mitochondrial membrane potential was evaluated by Rhodamine 123 fluorescence in larval muscles. Third-instar larvae were dissected in HL3 and incubated in the same buffer in the presence of 20 μM Rhodamine 123 for 15 min at room temperature. Before imaging, larvae were washed three times with HL3, and 20 mM glutamate was added. Fluorescence was recorded before (F_0) and 5 min after carbonyl cyanide 4-(trifluoromethoxy)phenylhydrazone (FCCP, 50 μm) addition (F_{FCCP}). Background fluorescence was measured in nuclear areas devoid of mitochondria and subtracted from both F_0 and F_{FCCP}. Fluorescence values for each genotype were calculated as $F_0 - F_{FCCP}$ and normalized to controls.

Mitochondrial Respiration Assay

Oxygen consumption measurements were performed using a Clark-type electrode (Hansatech Instruments, King's Lynn, England). An equal weight of larvae was cut up and added to 1 mL of respiration buffer (120 mM sucrose, 4 mM KH_2PO_4, 50 mM KCl, 4 mM $MgCl_2$, 1 mM EGTA, 0.01% digitonin, and 20 mM TRIS-Cl [pH 7.4]) at room temperature. Total oxygen consumption was calculated by subtracting the rate measured under physiological conditions with that measured after addition of 5 μM Rotenone and 5 μM Antimycin A. Mitochondrial respiration was normalized to total larvae weight.

Mitochondrial ATP Synthesis

The rate of ATP synthesis was measured in isolated mitochondria from third-instar larvae. Briefly, an equal weight of larvae was resuspended in ice-cold buffer containing 200 mM mannitol, 70 mM sucrose, 1 mM EGTA, 10 mM KH_2PO_4, 2 mM HEPES (pH 7.6), and 4 mg/ml BSA and mechanically disrupted with a glass/teflon Potter-Elvehjem homogenizer. Differential centrifugations (600 g for 10 min at 4°C followed by 14,000 × *g* for 20 min at 4°C) were performed to separate crude mitochondria, and samples were used for measurement immediately. The rate of mitochondrial ATP synthesis was measured with the luciferin/luciferase assay in a buffer containing 150 mM KCl, 25 mM Tris-Cl, 2 mM EDTA, 0.1% BSA, 10 mM KH_2PO_4, and 0.1 mM $MgCl_2$ (pH 7.4) at 25°C. 200–400 μg of crude mitochondria were incubated in the same buffer in the presence of 1 mM malate and 1 mM pyruvate. After the addition of 0.2 mM ADP, chemiluminescence was determined as a function of time with a luminometer (Berthold, Sirius-L). The chemioluminescence signal was calibrated with an internal ATP standard after addition of 1 μM oligomycin. The rates of ATP synthesis were normalized to protein content and citrate synthase (CS) activity (Trounce et al., 1996).

Mitochondrial Motility Assay

Third-instar larvae were dissected quickly (<5 min) in PBS 1× in the presence of 7 mM glutamate, and GFP-tagged mitochondria were imaged along segmental nerves using a confocal microscope equipped with a 60× water Fluor objective (Nikon). To allow for accurate long-range tracking of mitochondrial transport, we photobleached a 40-μm region of the segmental nerve 30 times with a 488-nm laser at full intensity. Immediately after photobleaching, images were collected at a rate of one frame every 2 s for 100 times. Recordings were collected from specimens within 40 min of the start of dissection, and a maximum of three time-lapse recordings was acquired from each larva.

Co-immunoprecipitation

S2 cells were transfected using Mirus TransIt Insect with plasmids encoding Marf-myc and dMiro-EGFP or atlastin-myc and atlastin-EGFP. Cells were lysed in ice-cold RIPA buffer (50 mM Tris, 150 mM NaCl, 1% Triton X-100, 0.5% deoxycholic acid, 0.1% SDS, and protease inhibitor cocktail [pH 7.5]) for 30 min and clarified by spinning at 13,000 rpm for 15 min. Protein concentration was determined using the Advanced Protein Assay Reagent #2 (Cytoskeleton). Immunoprecipitation was performed with anti-myc Magnetic Beads (Thermo Fisher). All fractions were boiled in Laemmli sample buffer before separation by SDS-PAGE. Western blot analysis was performed with rabbit anti-myc and anti-GFP antibodies (Cell Signaling, 1:1,000).

Electron Microscopy

Drosophila thoraxes were fixed in 4% paraformaldehyde and 2% glutaraldehyde and embedded as previously described (Yang et al., 2006). EM images were acquired from thin sections under a FEI Tecnai-12 electron microscope.

Statistics

All data are representative of at least three experiments. Image analysis was performed using Volocity (PerkinElmer) and ImageJ (NIH). Unless otherwise stated, numerical values presented throughout the text refer to mean ± SEM. n = number of independent experiments (larvae) or number of cells; *p < 0.05, **p < 0.01, ***p < 0.001, and ****p < 0.0001. Statistical significance for pairwise comparisons was evaluated with a two-tailed Student's t test.

SUPPLEMENTAL INFORMATION

Supplemental Information includes five figures and can be found with this article online at https://doi.org/10.1016/j.celrep.2018.04.017.

ACKNOWLEDGMENTS

This work was supported by a 5x1000 grant from the Italian Ministry of Health (to A.D.) and a Starting Grant 2015 from Cariparo Foundation (to D.P.).

AUTHOR CONTRIBUTIONS

Conceptualization, A.D., T.T., and D.P.; Methodology, A.D., T.T., D.P., and A.M.G.; Investigation, T.T., D.P., A.M., and A.G.; Writing – Original Draft, A.D.; Writing – Review & Editing, A.D., D.P., T.T., and A.G.; Funding Acquisition, A.D.; Resources, S.B.; and Supervision, A.D.

DECLARATION OF INTERESTS

The authors declare no competing interests.

Received: June 21, 2017
Revised: March 1, 2018
Accepted: April 2, 2018
Published: May 8, 2018

REFERENCES

Ashrafi, G., Schlehe, J.S., LaVoie, M.J., and Schwarz, T.L. (2014). Mitophagy of damaged mitochondria occurs locally in distal neuronal axons and requires PINK1 and Parkin. J. Cell Biol. *206*, 655–670.

Baloh, R.H., Schmidt, R.E., Pestronk, A., and Milbrandt, J. (2007). Altered axonal mitochondrial transport in the pathogenesis of Charcot-Marie-Tooth disease from mitofusin 2 mutations. J. Neurosci. *27*, 422–430.

Bertholet, A.M., Millet, A.M., Guillermin, O., Daloyau, M., Davezac, N., Miquel, M.C., and Belenguer, P. (2013). OPA1 loss of function affects in vitro neuronal maturation. Brain *136*, 1518–1533.

Brand, M.D., and Nicholls, D.G. (2011). Assessing mitochondrial dysfunction in cells. Biochem. J. *435*, 297–312.

Burté, F., Carelli, V., Chinnery, P.F., and Yu-Wai-Man, P. (2015). Disturbed mitochondrial dynamics and neurodegenerative disorders. Nat. Rev. Neurol. *11*, 11–24.

Cai, Q., Zakaria, H.M., Simone, A., and Sheng, Z.H. (2012). Spatial parkin translocation and degradation of damaged mitochondria via mitophagy in live cortical neurons. Curr. Biol. *22*, 545–552.

Chen, H., Detmer, S.A., Ewald, A.J., Griffin, E.E., Fraser, S.E., and Chan, D.C. (2003). Mitofusins Mfn1 and Mfn2 coordinately regulate mitochondrial fusion and are essential for embryonic development. J. Cell Biol. *160*, 189–200.

Chen, H., Chomyn, A., and Chan, D.C. (2005). Disruption of fusion results in mitochondrial heterogeneity and dysfunction. J. Biol. Chem. *280*, 26185–26192.

Debattisti, V., Pendin, D., Ziviani, E., Daga, A., and Scorrano, L. (2014). Reduction of endoplasmic reticulum stress attenuates the defects caused by Drosophila mitofusin depletion. J. Cell Biol. *204*, 303–312.

Jang, S., Nelson, J.C., Bend, E.G., Rodríguez-Laureano, L., Tueros, F.G., Cartagenova, L., Underwood, K., Jorgensen, E.M., and Colón-Ramos, D.A. (2016). Glycolytic enzymes localize to synapses under energy stress to support synaptic function. Neuron *90*, 278–291.

Lin, M.Y., and Sheng, Z.H. (2015). Regulation of mitochondrial transport in neurons. Exp. Cell Res. *334*, 35–44.

Louie, K., Russo, G.J., Salkoff, D.B., Wellington, A., and Zinsmaier, K.E. (2008). Effects of imaging conditions on mitochondrial transport and length in larval motor axons of Drosophila. Comp. Biochem. Physiol. A Mol. Integr. Physiol. *151*, 159–172.

Meeusen, S., DeVay, R., Block, J., Cassidy-Stone, A., Wayson, S., McCaffery, J.M., and Nunnari, J. (2006). Mitochondrial inner-membrane fusion and crista maintenance requires the dynamin-related GTPase Mgm1. Cell *127*, 383–395.

Miller, K.E., and Sheetz, M.P. (2004). Axonal mitochondrial transport and potential are correlated. J. Cell Sci. *117*, 2791–2804.

Misko, A., Jiang, S., Wegorzewska, I., Milbrandt, J., and Baloh, R.H. (2010). Mitofusin 2 is necessary for transport of axonal mitochondria and interacts with the Miro/Milton complex. J. Neurosci. *30*, 4232–4240.

Misko, A.L., Sasaki, Y., Tuck, E., Milbrandt, J., and Baloh, R.H. (2012). Mitofusin2 mutations disrupt axonal mitochondrial positioning and promote axon degeneration. J. Neurosci. *32*, 4145–4155.

Olichon, A., Baricault, L., Gas, N., Guillou, E., Valette, A., Belenguer, P., and Lenaers, G. (2003). Loss of OPA1 perturbates the mitochondrial inner membrane structure and integrity, leading to cytochrome c release and apoptosis. J. Biol. Chem. *278*, 7743–7746.

Pareyson, D., Saveri, P., Sagnelli, A., and Piscosquito, G. (2015). Mitochondrial dynamics and inherited peripheral nerve diseases. Neurosci. Lett. *596*, 66–77.

Rangaraju, V., Calloway, N., and Ryan, T.A. (2014). Activity-driven local ATP synthesis is required for synaptic function. Cell *156*, 825–835.

Sandoval, H., Yao, C.K., Chen, K., Jaiswal, M., Donti, T., Lin, Y.Q., Bayat, V., Xiong, B., Zhang, K., David, G., et al. (2014). Mitochondrial fusion but not fission regulates larval growth and synaptic development through steroid hormone production. eLife *3*, 3.

Scaduto, R.C., Jr., and Grotyohann, L.W. (1999). Measurement of mitochondrial membrane potential using fluorescent rhodamine derivatives. Biophys. J. *76*, 469–477.

Schon, E.A., and Przedborski, S. (2011). Mitochondria: the next (neurode)generation. Neuron *70*, 1033–1053.

Sheng, Z.H. (2014). Mitochondrial trafficking and anchoring in neurons: new insight and implications. J. Cell Biol. *204*, 1087–1098.

Spinazzi, M., Cazzola, S., Bortolozzi, M., Baracca, A., Loro, E., Casarin, A., Solaini, G., Sgarbi, G., Casalena, G., Cenacchi, G., et al. (2008). A novel deletion in the GTPase domain of OPA1 causes defects in mitochondrial morphology and distribution, but not in function. Hum. Mol. Genet. *17*, 3291–3302.

Trounce, I.A., Kim, Y.L., Jun, A.S., and Wallace, D.C. (1996). Assessment of mitochondrial oxidative phosphorylation in patient muscle biopsies, lymphoblasts, and transmitochondrial cell lines. Methods Enzymol. *264*, 484–509.

Verburg, J., and Hollenbeck, P.J. (2008). Mitochondrial membrane potential in axons increases with local nerve growth factor or semaphorin signaling. J. Neurosci. *28*, 8306–8315.

Verstreken, P., Ly, C.V., Venken, K.J., Koh, T.W., Zhou, Y., and Bellen, H.J. (2005). Synaptic mitochondria are critical for mobilization of reserve pool vesicles at Drosophila neuromuscular junctions. Neuron *47*, 365–378.

Wai, T., and Langer, T. (2016). Mitochondrial dynamics and metabolic regulation. Trends Endocrinol. Metab. *27*, 105–117.

Westermann, B. (2008). Molecular machinery of mitochondrial fusion and fission. J. Biol. Chem. *283*, 13501–13505.

Westermann, B. (2012). Bioenergetic role of mitochondrial fusion and fission. Biochim. Biophys. Acta *1817*, 1833–1838.

Yang, Y., Gehrke, S., Imai, Y., Huang, Z., Ouyang, Y., Wang, J.W., Yang, L., Beal, M.F., Vogel, H., and Lu, B. (2006). Mitochondrial pathology and muscle and dopaminergic neuron degeneration caused by inactivation of Drosophila Pink1 is rescued by Parkin. Proc. Natl. Acad. Sci. USA *103*, 10793–10798.

Yarosh, W., Monserrate, J., Tong, J.J., Tse, S., Le, P.K., Nguyen, K., Brachmann, C.B., Wallace, D.C., and Huang, T. (2008). The molecular mechanisms of OPA1-mediated optic atrophy in Drosophila model and prospects for antioxidant treatment. PLoS Genet. *4*, e6.

Yu, T., Wang, L., and Yoon, Y. (2015). Morphological control of mitochondrial bioenergetics. Front. Biosci. *20*, 229–246.

Yu, Y., Lee, H.C., Chen, K.C., Suhan, J., Qiu, M., Ba, Q., and Yang, G. (2016). Inner membrane fusion mediates spatial distribution of axonal mitochondria. Sci. Rep. *6*, 18981.

Zorzano, A., Liesa, M., Sebastián, D., Segalés, J., and Palacín, M. (2010). Mitochondrial fusion proteins: dual regulators of morphology and metabolism. Semin. Cell Dev. Biol. *21*, 566–574.